buildings

MDPI

Article

EICP Surface Spraying Reinforcement of Yan'an Q3 Loess: Optimization and Pore-Scale Mechanism

Xueyan Wang [1], Guojie Dong [1,*], Yili Yuan [2], Tao Yang [1], Bo Wang [1] and Mengyuan Liu [1]

[1] School of Urban Planning and Municipal Engineering, Xi'an Polytechnic University, Xi'an 710600, China; wxy19860412@163.com (X.W.); yangtao0604@163.com (T.Y.); 231421024@stu.xpu.edu.cn (B.W.); 231421032@stu.xpu.edu.cn (M.L.)

[2] School of Architecture and Civil Engineering, Xi'an University of Science and Technology, Xi'an 710054, China; yiliyuan@xauat.edu.cn

* Correspondence: 241421021@stu.xpu.edu.cn

Abstract

Surface erosion of loess slopes in arid and semi-arid regions of China remains a critical geotechnical issue, requiring green and low-carbon stabilization techniques. This study investigated the effectiveness of enzyme-induced carbonate precipitation (EICP) for the surface spraying reinforcement of Q3 loess collected from a high-fill engineering site at Yan'an University. Single-factor tests, response surface methodology (RSM), surface strength tests, CT-based three-dimensional pore reconstruction, and scanning electron microscopy (SEM) were conducted to evaluate the effects of cementation solution concentration and spraying dosage. The cementation solution was prepared by mixing analytical-grade urea and anhydrous calcium chloride at a 1:1 molar ratio, and the specimens were compacted to a dry density of 1.4 g/cm^3. The results showed that surface strength first increased and then decreased with increasing cementation solution concentration and spraying dosage. Spraying dosage had a more pronounced influence than cementation solution concentration; excessive spraying above 9 L/m^2 reduced surface strength because of the high water sensitivity of loess. Five replicate tests at the central point were conducted to evaluate experimental error. The optimal parameters were 1.5 mol/L for cementation solution concentration and 9 L/m^2 for spraying dosage. CT and SEM results showed that $CaCO_3$ precipitation filled large pores and cemented soil particles, reducing total porosity from 6.7% to approximately 4.0%. These findings indicate that EICP improves loess surface strength mainly through pore filling and particle cementation, providing guidance for the ecological protection of loess slopes.

Keywords: loess slope; EICP; surface strength; CT

Check for updates

Academic Editor: Bingxiang Yuan

Received: 6 May 2026
Revised: 21 June 2026
Accepted: 22 June 2026
Published: 23 June 2026

Copyright: © 2026 by the authors. Licensee MDPI, Basel, Switzerland. This article is an open access article distributed under the terms and conditions of the Creative Commons Attribution (CC BY) license.

1. Introduction

Loess is widely distributed in the arid and semi-arid regions of central and western China. Owing to its metastable structure, large pores, and high water sensitivity, the surface layer of loess slopes is prone to erosion and shallow collapse under rainfall, freeze–thaw cycles, and other environmental actions, posing a long-term threat to infrastructure safety [1–3]. In engineering practice, conventional slope reinforcement measures, including anti-slide piles, retaining walls, and prestressed anchor cables, have been widely adopted [4]. Cement- and lime-based treatments, such as cement mixing piles, are also commonly used to improve soil strength. However, these methods often involve high energy

consumption and carbon emissions during material production [5,6]. Their field application may also require long construction periods, cause considerable ecological disturbance, and change the soil chemical environment [7]. Therefore, developing green, low-carbon, and efficient technologies for slope surface protection and ecological reinforcement is of practical importance for engineering construction in loess regions [8].

In this context, enzyme-induced carbonate precipitation (EICP) has attracted increasing attention as a promising biomineralization technique for sustainable soil improvement. EICP uses plant-derived urease to catalyze urea hydrolysis and induce calcium carbonate precipitation, thereby cementing soil particles. Owing to its environmentally friendly raw materials, controllable reaction process, and relatively low energy consumption [9], EICP offers a potential approach for the sustainable reinforcement of loess slopes.

Nevertheless, the generation of ammonium ions (NH_4^+) as a by-product remains an important sustainability concern in EICP treatment. Excessive NH_4^+ accumulation may inhibit urease activity and adversely affect soil structure [10]. Therefore, controlling reactant input is essential for improving reinforcement efficiency while reducing the risk of by-product accumulation. In this study, this issue is addressed by optimizing cementation solution concentration and spraying dosage, with the aim of achieving effective surface spraying reinforcement under controlled material input.

Engineering application of EICP requires a clear understanding and continuous optimization of its key processes, particularly urease extraction and activity preservation. Previous studies have mainly examined enzyme source selection, extraction conditions, and activity preservation. Wang et al. [11] reported that sword bean urease exhibited a greater increase in activity after freezing at −20 °C than commonly used soybean urease, indicating that sword bean may be an efficient and cost-effective plant-derived enzyme source. Chen and Hazarika [12] further investigated the effects of soybean particle size, powder concentration, pH, temperature, and storage conditions on urease extraction efficiency and enzyme activity for low-cost and large-scale urease preparation. Their results showed that medium-sized soybean particles achieved a relatively high powder screening yield and favorable economic feasibility. Urease activity reached its maximum at pH 8, and storage at 4 °C effectively maintained enzyme activity for 72 h, providing practical guidance for low-cost urease preparation in EICP applications.

Lai et al. [13,14] further investigated the extraction of plant-derived and bacterial urease. They optimized soybean urease extraction using a water–ethanol mixed solution. For bacterial urease, they proposed an optimized ultrasonic extraction protocol to reduce extraction inefficiency and activity loss, with an upper temperature limit of 50 °C, a vibration amplitude of 69 μm, and continuous cooling. Their results showed that, when enzyme activity was maintained at a constant level, the extraction parameters had no significant effect on mineralization-induced soil improvement. These findings provide useful guidance for efficient enzyme preparation in EICP treatment.

In terms of injection strategies and reaction control, previous studies have mainly focused on reducing non-uniform reinforcement and pore clogging caused by excessively rapid EICP reactions. Ren et al. [15] proposed a method combining highly active urease with a high-concentration cementation solution to enhance calcium carbonate precipitation and improve the reinforcement of fine-grained soils. This method helps overcome the limitations of conventional low-concentration treatments in low-permeability soils. Cui et al. [16,17] investigated the grouting uniformity and urease stability of EICP treatment. They first proposed a one-phase low-pH EICP method, which effectively reduced pore clogging and non-uniform reinforcement during grouting. An improved process was then developed using a low-pH cementation solution instead of a low-pH urease solution, thereby avoiding urease inactivation under acidic conditions. Appropriate control thresholds for pH and

cementation solution concentration were also identified, improving both the controllability of mineralization and the uniformity of reinforcement. Meng et al. [18] developed a multi-phase EICP injection method, in which an enzyme–cementation solution mixture was first injected, followed by several rounds of cementation solution injection. This method increased urease utilization by at least four times and effectively alleviated clogging near the injection inlet. Overall, these studies provide useful references for improving the efficiency, controllability, and uniformity of EICP-based soil reinforcement.

With the continued development of EICP, its applications and EICP-based composite treatments have expanded to various engineering scenarios. For soil and backfill reinforcement, EICP has been used not only to treat sandy soils but also to improve the integrity and impermeability of pea gravel backfill layers behind TBM tunnel linings [19,20]. EICP also shows potential for repairing engineering materials and structures. Xie et al. [21] reported that combining EICP with lignin for concrete crack repair led to greater recovery of compressive and flexural strength, mainly because lignin provided abundant nucleation sites and promoted calcite formation. Similarly, EICP combined with biopolymers, such as sodium alginate and chitosan, improved the impermeability of repaired concrete by promoting calcium carbonate deposition and adhesion [22]. For loess, Chen et al. [23] confirmed that microbially induced carbonate precipitation (MICP) can improve the mechanical strength and water stability of loess, while Pan et al. [24] demonstrated the effectiveness of MICP in restoring the mechanical properties of fissured loess. These studies indicate that biomineralization techniques have broad material adaptability and engineering potential.

However, for the large-scale surface anti-erosion reinforcement of loess slopes, existing studies remain limited in terms of target specificity, process optimization, and mechanistic understanding. In particular, few studies have examined how cementation solution concentration and spraying dosage control the surface strength of EICP-treated loess. Although Wang et al. [11] demonstrated that combining EICP with nano-SiO_2 and soil stabilizer significantly enhanced loess surface strength, reaching 6.40 MPa at a dry density of 1.6 g/cm^3, their optimization focused on material ratios, such as nano-SiO_2 content and stabilizer dosage, rather than the joint control of cementation solution concentration and spraying dosage. Most parameter optimization studies have relied on single-factor tests [25], which cannot fully reveal the interaction between cementation solution concentration and spraying dosage under surface spraying conditions. Spraying dosage is especially important because it controls the thickness of the reinforced layer, material consumption, and the moisture state of the surface soil. However, its optimal threshold and the adverse effects of excessive spraying, such as over-wetting and structural softening of loess, remain unclear.

In addition, although microstructural characterization techniques have advanced rapidly, the relationship between pore-scale structural evolution and macroscopic surface strength remains insufficiently understood for EICP-treated loess surfaces. For example, Yu et al. [26] used μXCT combined with FIB-SEM to reveal the natural microstructure of loess. Luo et al. [27] proposed a CT image-based method for microstructure quantification and numerical modeling. Huang et al. [28] used micro-CT to clarify pore structure deterioration under drying–wetting cycles, and Wang et al. [29] showed that the chemical composition of the cementation solution, such as Mg^{2+}, can affect macroscopic strength by changing the morphology of calcium carbonate crystals. Nevertheless, systematic understanding remains limited regarding how process parameters regulate the three-dimensional pore network of EICP-treated loess surfaces, including the proportions of large, medium, and small pores, and how these changes further influence macroscopic surface strength. This knowledge gap limits the precise design and optimization of EICP treatment for loess slope protection.

To address these research gaps, this study systematically investigates an EICP-based surface spraying method for the reinforcement of Yan'an Q3 loess. The objectives of this study are to: (1) examine the individual and combined effects of cementation solution concentration and spraying dosage on the surface strength of EICP-treated loess using response surface methodology (RSM), and determine the optimal combination of treatment parameters; (2) classify and quantify the three-dimensional pore structure using CT scanning, together with SEM observations and surface strength tests, to reveal the pore-scale mechanisms by which EICP improves surface strength; and (3) clarify the influence patterns and threshold effects of the key treatment parameters. The findings are expected to provide theoretical support and process guidance for the field application of EICP in the ecological protection of loess slopes. Unlike conventional EICP grouting for deep soil improvement, this study focuses on surface spraying reinforcement. Its novelty lies in identifying the spraying dosage threshold governed by the high water sensitivity of loess and revealing the pore filling mechanism quantified by CT.

2. Materials and Methods

2.1. Loess

The loess used in this study was obtained from a high-fill engineering site at Yan'an University. It is a typical Q_3 silty clay with a loose structure and a light gray color. Its basic physical properties were determined according to GB/T 50123–2019 [30] (Table 1), and the grain-size distribution curve is shown in Figure 1.

Table 1. Basic physical property indexes of Loess.

Name of Soil Sample	Plastic Limit/%	Liquid Limit/%	Plasticity Index	Maximum Dry Density/(g/cm^3)	Optimum Moisture Content/%
Q3 Loess	18.3	29.6	11.4	1.78	16.9

Note: The maximum dry density and optimum moisture content were determined according to the light compaction test (Standard Proctor) specified in GB/T 50123-2019, corresponding to a compaction energy of 592.2 kJ/m^3.

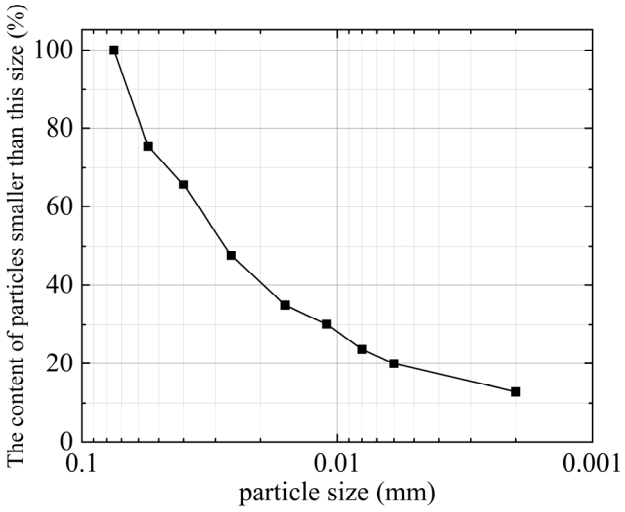


Figure 1. Gradation curve of the tested loess.

2.2. Urease

Commercially available sword beans were used as the raw material for urease extraction. The extraction procedure was as follows: (1) the sword beans were dried in an oven at 50 °C for 8 h; (2) the dried sword beans were ground into powder using a grinder and passed through a 100-mesh sieve; (3) the sieved bean powder was frozen at −20 °C for

24 h [31]; (4) a 100 g/L bean powder solution was prepared with deionized water and centrifuged at 3000 rpm for 20 min to obtain the supernatant; and (5) the supernatant was filtered through a coarse mesh screen to remove surface foam and large debris. This filtration step was performed to prevent nozzle clogging during the subsequent spraying process, and the filtered solution was stored in a beaker for immediate use.

The urease activity of the prepared 100 g/L sword bean solution, after freezing at −20 °C for 24 h, was determined to be 27.29 μmol/min using the conductivity method [11], ensuring consistent enzymatic hydrolysis capacity across all experimental groups. The detailed steps are illustrated in Figure 2.

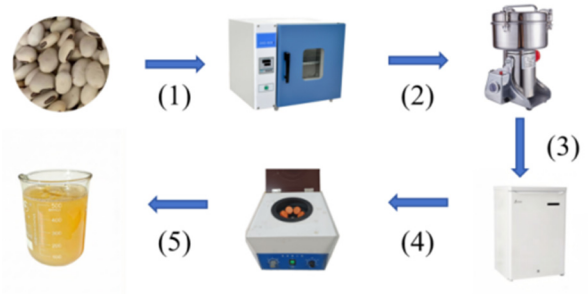


Figure 2. Extraction process of sword bean urease.

2.3. EICP Reaction Cementation Solution

Urea and anhydrous calcium chloride were analytical-grade reagents with a purity of ≥99% and were supplied by Tianmao Baoding Biotechnology Co., Ltd., Xi'an, China. The cementation solution was prepared by dissolving urea and anhydrous calcium chloride in deionized water at a 1:1 molar ratio. Both the cementation solution and the urease solution were freshly prepared before each test to ensure consistent cementation effectiveness.

2.4. Specimen Preparation and Curing

The loess was oven-dried, and its moisture content was adjusted to 16.5%—within the optimum moisture content range. After being sealed and conditioned for 24 h, the soil was passed through a 2 mm sieve. Specimens with dimensions of 195 mm × 175 mm × 30 mm were prepared via layered compaction using a custom-fabricated acrylic mold. To evaluate the surface strength enhancement of under-compacted loess following EICP treatment, the dry density was controlled at 1.4 g/cm^3.

The reaction solutions were manually sprayed using a handheld atomizing spray bottle. The same operator applied the reaction solutions until the specimen surface was visually moist, without ponding or runoff. The total volume was strictly controlled according to the designed spraying dosage, such as 9 L/m^2, rather than the instantaneous spraying rate.

After spraying, the treated specimens were maintained under natural ventilation in an indoor environment to simulate the exposure conditions of field-applied surface spraying reinforcement. This initial curing phase lasted 7 d to allow sufficient time for enzymatic hydrolysis and initial calcium carbonate precipitation.

After this period, the moisture content of all specimens was uniformly adjusted to 15% using the weighing method to standardize the initial conditions. The specimens were then individually wrapped with cling film to prevent moisture exchange and transferred to a constant temperature and humidity chamber at 20 °C and 95% RH for an additional 2 d of curing. This final curing stage ensured a stable and consistent microstructural state across all specimens before mechanical testing.

2.5. Experimental Plan

2.5.1. Experimental Design

Cementation solution concentration and spraying dosage were selected as the two controlled factors for the single-factor surface strength tests and were denoted as Factor A and Factor B, respectively. The levels of cementation solution concentration were 0.5, 1.0, 1.25, and 1.5 mol/L, while the levels of spraying dosage were 5, 7, 9, and 11 L/m^2. A plain soil control group was also included. Based on this experimental design, a total of 17 specimen groups were prepared.

2.5.2. Surface Strength Test

The surface strength test was designed to simulate shallow erosion and surface exfoliation of loess slopes under rainfall impact and runoff. Surface strength was measured using a digital push–pull force gauge equipped with a conical probe with a diameter of 10 mm. The testing setup is shown in Figure 3. To minimize boundary effects, the measurement points were arranged at a certain distance from the specimen edge, as shown in Figure 4. During the test, the probe was advanced at a rate of 1 mm/s until a penetration depth of 1 cm was reached, which was consistent with the near-surface damage zone considered in this study [11].

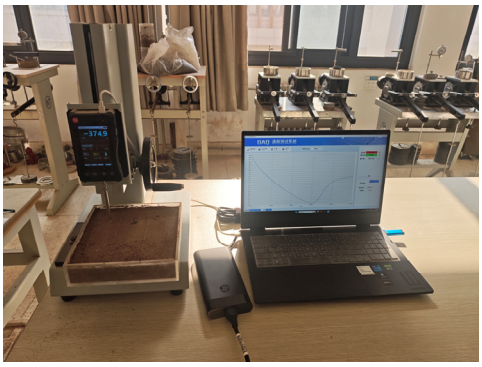


Figure 3. Digital push–pull force gauge.

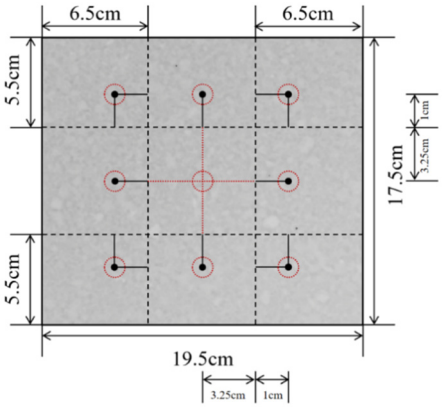


Figure 4. The locations of the measurement points for surface strength.

For the single-factor tests, one specimen was prepared for each test condition (n = 1). For the response surface tests, one specimen was prepared for each design point, except for the central point, where five independent specimens were prepared to evaluate reproducibility and pure error (n = 5).

For each specimen, nine measurement points were evenly distributed across the specimen surface while avoiding the boundaries to reduce the influence of local heterogeneity.

The average value of the nine measurements was taken as the representative surface strength of that specimen.

2.5.3. Microscopic Test

The CT scanning test was conducted on the high-performance CT testing platform at Xi'an University of Science and Technology using a nanoVoxel 2000 high-resolution X-ray micro-CT system (Sanying Precision Instruments Co., Ltd., Tianjin, China). The scanning voltage and tube current were set to 115 kV and 0.28 mA, respectively, to ensure sufficient penetration and imaging clarity.

The CT specimens were standard cylindrical specimens with a diameter of 41 mm and a height of 30 mm. The procedures for specimen preparation, dry density control, reaction solution spraying, and curing were consistent with those used in the surface strength test. Based on the surface strength test results, the CT test was conducted at a dry density of 1.40 g/cm^3 as the standard control condition, including a plain soil control group and an EICP reinforcement group. In the EICP reinforcement group, the spraying dosage was fixed at 9 L/m^2, and the cementation solution concentrations were set to 0, 0.5, 1.0, 1.25, 1.5, and 1.75 mol/L, resulting in six specimen groups.

To improve CT image quality and reduce the influence of moisture on X-ray attenuation, all CT specimens were naturally air-dried before scanning. Meanwhile, surface soil samples were collected from the specimens used in the surface strength test to prepare standard specimens for SEM observation. Scanning electron microscopy (SEM) was then used to analyze the microscopic morphology, calcium carbonate formation characteristics, and pore structure evolution of EICP-treated loess.

3. Results and Discussion

3.1. Analysis of Surface Strength Test Results

3.1.1. Single Factor Analysis

To optimize the EICP treatment process, this section analyzes the individual effects of cementation solution concentration and spraying dosage on surface strength. The experimental results are shown in Figures 5 and 6.

1. The influence of cementation solution concentration

When the cementation solution concentration was 0.5 mol/L, the overall surface strength showed only limited improvement, even with an increased spraying dosage. This was mainly attributed to the insufficient supply of urea and Ca^{2+}, which limited the amount of $CaCO_3$ precipitation produced by the EICP reaction. As a result, the generated $CaCO_3$ was insufficient to effectively fill loess pores and cement soil particles.

Under the same spraying dosage, surface strength increased markedly as the cementation solution concentration increased from 0.5 mol/L to 1.5 mol/L, reaching a peak at 1.5 mol/L (Figure 6). The peak surface strength was 2.08 times that of the untreated plain soil, indicating that an adequate supply of Ca^{2+} and carbonate ions promoted $CaCO_3$ precipitation and enhanced the mineralization-induced reinforcement effect. However, a further increase in cementation solution concentration did not produce additional strength improvement. In the subsequent response surface tests, when the spraying dosage was fixed at 7 L/m^2, increasing the cementation solution concentration to 1.75 mol/L resulted in a surface strength 0.13 MPa lower than that obtained at 1.25 mol/L. This reduction may be attributed to the inhibitory effect of excessive Ca^{2+} and urea on urease activity, which reduced the efficiency of $CaCO_3$ precipitation and weakened the reinforcement effect.

2. The influence of reaction solution spraying dosage.

At the same cementation solution concentration, increasing the spraying dosage from 5 L/m^2 to 9 L/m^2 led to a continuous increase in surface strength. This indicates that a higher spraying dosage promotes the formation of more $CaCO_3$ precipitation and allows the reaction solution to penetrate deeper into the surface soil, thereby enhancing the cementation effect.

However, when the spraying dosage reached 11 L/m^2, surface strength decreased markedly in all specimen groups. This decrease was mainly attributed to excessive spraying, which increased the soil moisture content, reduced the effective stress between soil particles, and caused structural softening and loosening. These effects limited stable $CaCO_3$ cementation. In addition, the combined effect of high moisture content and high cementation solution concentration may have promoted NH_4^+ accumulation in the system, increased pH, further inhibited urease activity, reduced the efficiency of $CaCO_3$ precipitation, and ultimately weakened the reinforcement effect.

In summary, both cementation solution concentration and spraying dosage significantly affected surface strength. Spraying dosage showed a distinct threshold of approximately 9 L/m^2. Exceeding this threshold reduced surface strength because of the high water sensitivity of loess.

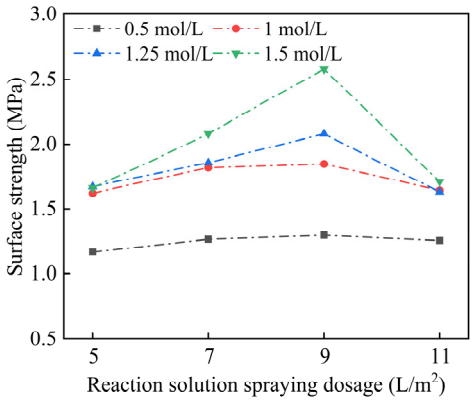


Figure 5. Effect of cementing solution concentration and reaction solution spraying dosage on surface strength.

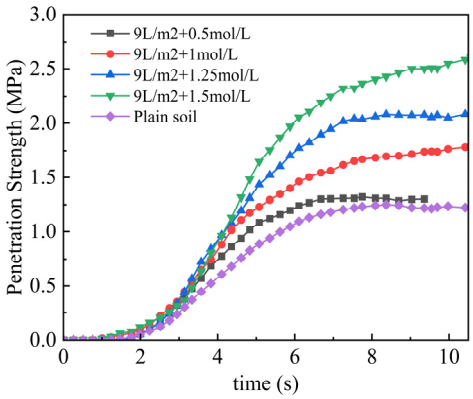


Figure 6. Penetration intensity changes with time.

3.1.2. Response Surface Modeling and Influence Analysis

Based on the single-factor test results, response surface analysis was conducted using the Central Composite Design module in Design-Expert (v13) software. Cementation solution concentration (A) and spraying dosage (B) were selected as the independent variables, while surface strength (F) was used as the response variable. To estimate experimental error,

five replicate tests were performed only at the central point (A = 1.5 mol/L, B = 9 L/m^2). The experimental data are shown in Table 2.

Table 2. Response surface design and results.

Order Number		1	2	3	4	5	6	7	8	9	10	11	12	13
Response factor	A mol/L	1.25	1.75	1.25	1.75	1.14645	1.85355	1.5	1.5	1.5	1.5	1.5	1.5	1.5
	B L/m^2	7	7	11	11	9	9	6.17157	11.8284	9	9	9	9	9
Response value	F MPa	1.86	1.73	1.63	1.48	2.06	1.71	1.92	1.56	2.56	2.43	2.7	2.58	2.65

A multiple regression model was established by fitting the response surface test data to describe the relationship among cementation solution concentration, spraying dosage, and surface strength.

$$F = 2.58 - 0.0969 * A - 0.1236 * B - 0.005 * AB - 0.3839 * A^2 - 0.4564 * B^2 \quad (1)$$

Analysis of variance (ANOVA) was used to evaluate the significance of the linear, interaction, and quadratic terms in the response surface model. The ANOVA results are shown in Table 3. The p-value was used to determine the significance level of each term, with $p < 0.05$ indicating significance (*) and $p < 0.01$ indicating high significance (**). Based on the F-values, the relative influence of the two factors on the surface strength of EICP-treated specimens followed the order: spraying dosage > cementation solution concentration. The quadratic terms A^2 and B^2 were highly significant, indicating that cementation solution concentration and spraying dosage had nonlinear effects on surface strength. In contrast, the interaction term AB was not significant ($p = 0.9306$), suggesting a weak interaction between the two factors. The overall model was highly significant ($p < 0.0001$), while the lack of fit was not significant ($p = 0.3692 > 0.05$). The coefficient of determination ($R^2 = 0.9654$) indicated good agreement between the model and the experimental data. The adjusted coefficient of determination (Adjusted $R^2 = 0.9406$) showed that 94.06% of the variability in the experimental data could be explained by the regression model. Figure 7 compares the measured and predicted values of the response surface model. The data points were distributed close to the diagonal line, further confirming the good fitting performance of the model.

Table 3. Variance analysis of surface strength response surface.

Source	Sum of Squares	Degree of Freedom	Mean Square	*F*-Value	*p*-Value	Significance
Model	2.39	5	0.4782	39.00	<0.0001	**
A	0.751	1	0.0751	6.12	0.0425	*
B	0.1223	1	0.1223	9.98	0.0160	*
AB	0.0001	1	0.0001	0.0082	0.9306	
A^2	1.03	1	1.03	83.62	<0.0001	**
B^2	1.45	1	1.45	118.19	<0.0001	**
Residual	0.0858	7	0.0123			
Lack of Fit	0.0437	3	0.0146	1.38	0.3692	
Pure Error	0.0421	4	0.0105			
Cor Total	2.48	12				

Note: $p < 0.05$ indicating significance (*) and $p < 0.01$ indicating high significance (**).

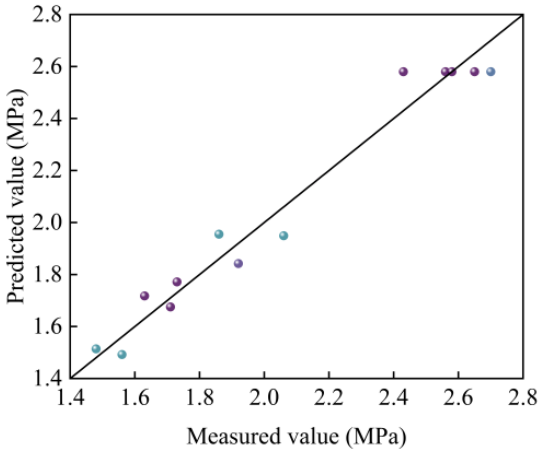


Figure 7. Comparison of the measured value with the predicted value.

To further illustrate the combined effects of cementation solution concentration and spraying dosage, response surface and contour plots were generated using Design-Expert software, as shown in Figure 8. As can be seen from Figure 8, surface strength first increased and then decreased with increasing cementation solution concentration and spraying dosage. The peak of the response surface was located near the central region of the design space, and the predicted optimal parameter combination was determined as A (cementation solution concentration) = 1.5521 mol/L and B (spraying dosage) = 9.22679 L/m^2.

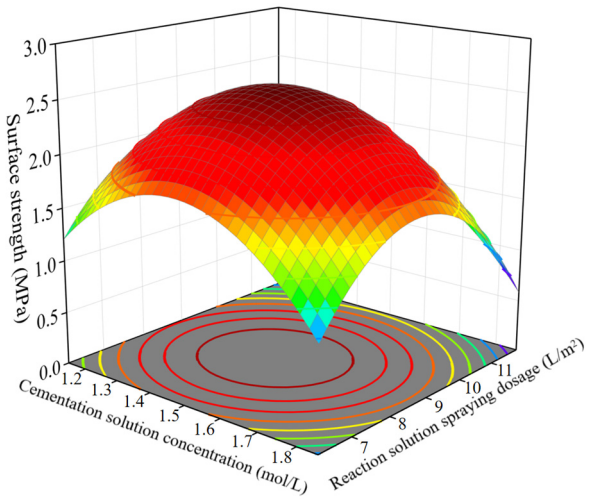
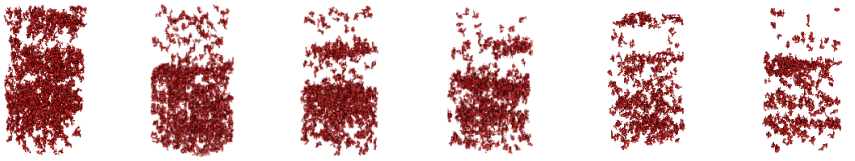
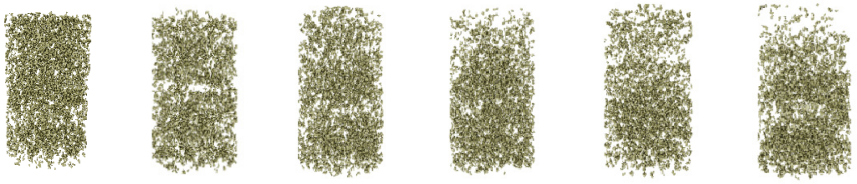
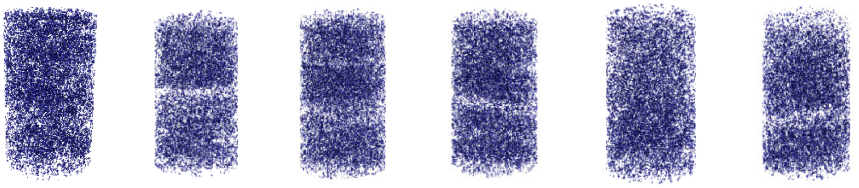


Figure 8. Interaction effects of the factors.

3.2. Analysis of CT Results

CT scanning was performed on the CT specimens, and the scanned data were reconstructed in three dimensions using Avizo (v2024.2) software. The pores were classified into three categories according to pore volume: large pores ($V > 8 \times 10^7$ μm^3), medium pores (1×10^7 μm^3 < $V < 8 \times 10^7$ μm^3), and small pores ($V < 1 \times 10^7$ μm^3). The three-dimensional visualization of pore structure evolution is presented in Table 4, providing a direct comparison of pore distribution under different cementation solution concentrations. Correspondingly, Figure 9 quantitatively presents the proportions of large, medium, and small pores, as well as the total porosity.

Table 4. 3D pore reconstruction of CT-scanned samples.

Cementation Solution Concentrations	0 mol/L	0.5 mol/L	1 mol/L	1.25 mol/L	1.5 mol/L	1.75 mol/L
large pore						
medium pore						
small pore						

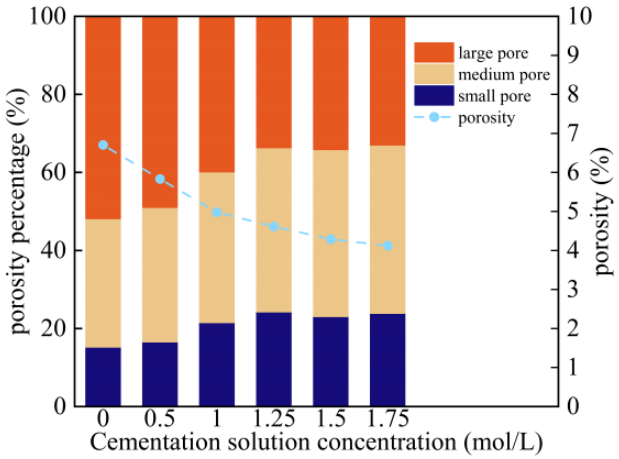


Figure 9. Effect of different cementation solution concentrations on soil pores.

Micro-CT images were processed to segment pores from the solid matrix. The total porosity (ϕ) was then quantified by calculating the volume fraction of the identified pore regions within the entire 3D dataset. The calculation was performed using the following formula:

$$\phi = \frac{V_{\text{pore}}}{V_{\text{bulk}}} \quad (2)$$

V_{pore}: Pore Volume, V_{bulk}: Bulk Volume.

As shown in Figure 9, under the same dry density and spraying dosage, the proportion of large pores gradually decreased with increasing cementation solution concentration, whereas the proportions of medium and small pores increased. This trend can be attributed to the greater space provided by large pores for reaction solution accumulation, which allowed the EICP reaction to occur preferentially in these pores. As a result, large pores were gradually filled or subdivided into medium and small pores. The total porosity decreased from 6.7% to approximately 4.0% and then tended to stabilize.

This phenomenon may be related to the preferential formation of $CaCO_3$ precipitation in the upper part of the specimen. The initially formed $CaCO_3$ precipitation may have

partially blocked the pore-throat channels in the upper layer, causing the EICP reaction to be concentrated mainly in the shallow soil layer. This also explains the variation pattern of large pores shown in Table 4: the number and proportion of large pores in the upper part decreased gradually with increasing cementation solution concentration, whereas the changes in the lower part were less pronounced.

In addition, pore structure refinement increased the contact area and interlocking effect between soil particles, thereby improving the structural stability and frictional resistance of the soil under loading. It may also help inhibit water infiltration and the development of internal seepage channels, providing a theoretical basis for slope surface protection. Overall, the three-dimensional reconstruction of pore structure further confirms the pore filling and particle cementation effects induced by $CaCO_3$ precipitation.

3.3. Analysis of SEM Results

The improvement in surface strength induced by EICP is mainly attributed to the in situ formation of $CaCO_3$ precipitation through urease-catalyzed reactions, which reinforces the soil structure. SEM observations were conducted on selected specimens after the surface strength tests, and the results are shown in Figures 10 and 11. As shown in Figure 11, when the cementation solution concentration increased from 0 mol/L to 1.5 mol/L, the amount of $CaCO_3$ precipitation increased, while soil porosity decreased markedly. This observation supports the macroscopic surface strength variation from a microscopic perspective. The EICP-induced improvement in surface strength can be mainly attributed to two mechanisms: pore filling and particle cementation.

1. As shown in Figure 11a, $CaCO_3$ precipitation filled and subdivided the larger pores in the soil, transforming connected pores into isolated smaller pores. As a result, the total porosity decreased from 6.7% to approximately 4.0%, corresponding to a reduction of about 40%, which indicates a marked improvement in soil compactness.
2. $CaCO_3$ precipitation preferentially adhered to the surfaces of soil particles. As the cementation solution concentration increased, $CaCO_3$ precipitation gradually developed from isolated attachments into inter-particle bonds, thereby reducing the gaps between soil particles and enhancing the stability of the soil structure, as shown in Figure 11b.

In summary, $CaCO_3$ precipitation improved the microstructure of loess through the combined effects of pore filling and particle cementation. These effects formed a denser and more integrated soil skeleton, ultimately contributing to the improvement in surface strength. This conclusion is consistent with the three-dimensional pore evolution revealed by CT reconstruction and the results of the surface strength tests.

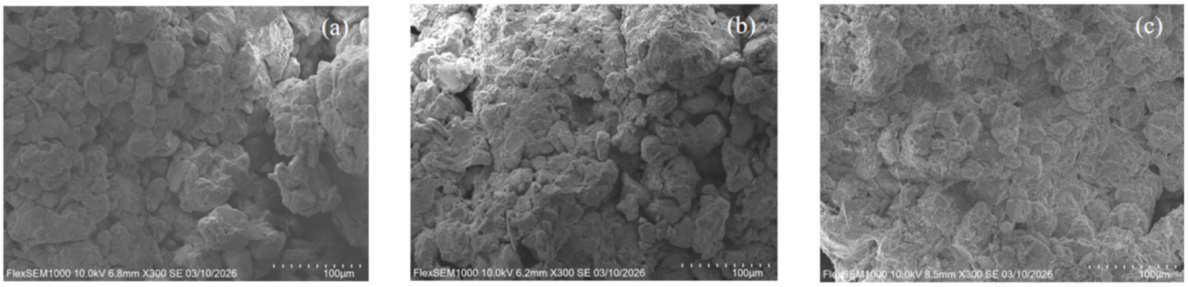


Figure 10. Effect of cementation solution concentration on $CaCO_3$ precipitation. (**a**) A = 0 (**b**) A = 1 (**c**) A = 1.5 concentration of the cementation solution (A).

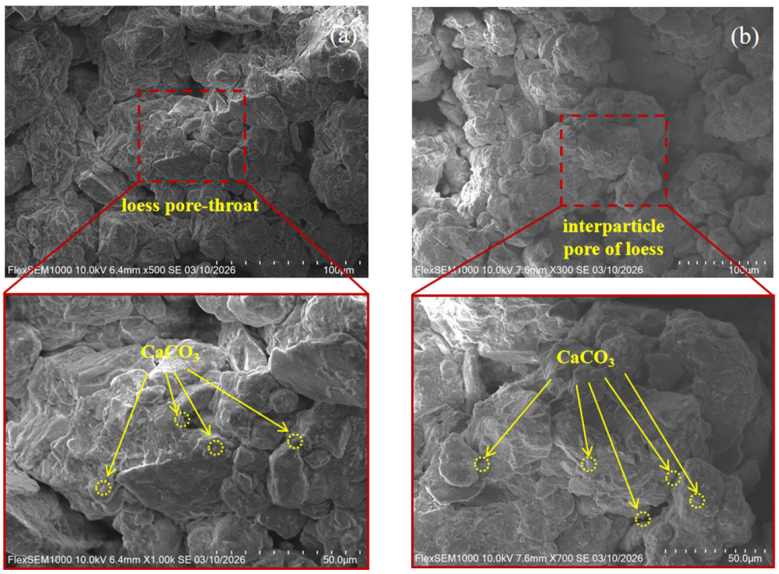


Figure 11. SEM images of EICP-treated samples. (**a**) soil pores (**b**) pores between soil particles.

4. Conclusions

This study investigated the effects of cementation solution concentration and spraying dosage on the surface strength and microstructure of loess treated by enzyme-induced carbonate precipitation (EICP), and further optimized the combination of these two parameters. First, single-factor tests were conducted to determine the individual effects of cementation solution concentration and spraying dosage on the surface strength of EICP-treated loess, based on which suitable value ranges for each factor were preliminarily identified. Subsequently, response surface methodology (RSM) was used to establish a response surface model and determine the optimal parameter combination. To further reveal the reinforcement mechanism, microstructural tests, including computed tomography (CT) scanning and scanning electron microscopy (SEM) observations, were conducted to analyze the modification of soil microstructure by EICP in terms of pore structure and microscopic morphology. The main conclusions are as follows:

1. Threshold effect of parameters: The surface strength of EICP-treated loess is governed by both cementation solution concentration and spraying dosage, with the latter exerting a more dominant influence. Due to the highwater sensitivity of loess, a distinct threshold for spraying dosage (9 L/m^2) was identified. Excessive spraying leads to structural softening and a subsequent reduction in strength.
2. Parameter optimization and economic feasibility: A strength prediction model was established based on the response surface methodology. Considering both reinforcement efficiency and economic feasibility, the optimal combination was determined to be a cementation solution concentration of 1.5 mol/L and a spraying dosage of 9 L/m^2. Under these conditions, the surface strength peaked at 2.08 times that of the untreated plain soil, achieving an optimal balance between reinforcement effect and material cost.
3. Pore structure evolution: Micro-CT results indicated that $CaCO_3$ precipitation preferentially filled large pores, dividing them into medium and small pores. Consequently, the total porosity decreased significantly from 6.7% to approximately 4.0%. This pore refinement enhanced inter-particle interlocking and friction, resulting in a denser soil skeleton.
4. Microscopic reinforcement mechanism: SEM analysis confirmed a dual mechanism of "pore filling" and "particle cementation." $CaCO_3$ crystals not only physically filled the

voids but also formed rigid cementation bridges between soil particles, transforming point contacts into surface contacts, thereby substantially improving macroscopic surface strength.

Author Contributions: Conceptualization: X.W. and G.D.; Methodology: X.W. and Y.Y.; Software: B.W.; Validation: Y.Y. and T.Y.; Formal analysis: T.Y.; Investigation: G.D. and M.L.; Resources: Y.Y.; Data curation: X.W. and B.W.; Writing—original draft preparation: G.D.; Writing—review and editing: X.W.; Visualization: M.L. and B.W.; Supervision: X.W. and Y.Y.; Project administration: B.W.; Funding acquisition: Y.Y. All authors have read and agreed to the published version of the manuscript.

Funding: This research was funded by the Youth Program of the National Natural Science Foundation of China (sponsored by the National Natural Science Foundation of China, Grant No. 52408393), Scientific Research and Development Project of the Department of Housing and Urban-Rural Development of Shaanxi Province (sponsored by the Department of Housing and Urban-Rural Development of Shaanxi Province, 2023-K46).

Data Availability Statement: The original data supporting the conclusion of this paper will be provided by the authors as needed.

Conflicts of Interest: The authors declare no conflicts of interest.

References

1. Liu, X.; Pan, C. Study on Micro-Characteristics of Microbe-Induced Calcium Carbonate Solidified Loess. *Crystals* **2021**, *11*, 1492.
2. Liu, J.; Ou, X. Mechanical Mechanism and Quantitative Analysis of Water Sensitivity of Loess. *Sci. Technol. Eng.* **2026**, *26*, 2104–2112.
3. Kong, J.; Deng, G. Dewater sensitivity of under-compacted saturated loess. *Hydrogeol. Eng. Geol.* **2026**, *53*, 158–170.
4. Ren, J.; Hu, S. Causes and reinforcement measures for expansive soil dangeroussituations of high slopes. *Chin. J. Geotech. Eng.* **2022**, *44*, 138–142.
5. Zhang, C.-L.; Jiang, G.-L. Effect of cement on the stabilization of loess. *J. Mt. Sci.* **2017**, *14*, 2325–2336. [CrossRef]
6. Liu, R.; Yan, S. Research on reinforced anchor with fibre mortar. *Chin. J. Geotech. Eng.* **2005**, *27*, 214–218.
7. Ou, Y.; Zhang, H. Optimization of the ratio of expansive soil improved by biological matrix based on response surface method. *Rock Soil Mech.* **2025**, *46*, 1368–1378.
8. Saif, A.; Cuccurullo, A. Advances in Enzyme Induced Carbonate Precipitation and Application to Soil Improvement: A Review. *Materials* **2022**, *15*, 950. [CrossRef] [PubMed]
9. Liu, Y.; Gao, Y. Evaluation of enzyme-induced carbonate precipitation using crude soybean urease during soil percolation. *Acta Geotech.* **2024**, *19*, 1571–1580.
10. Ahenkorah, I.; Rahman, M.M. A Review of Enzyme Induced Carbonate Precipitation (EICP): The Role of Enzyme Kinetics. *Sustain. Chem.* **2021**, *2*, 92–114. [CrossRef]
11. Wang, X.; Wang, B. Study on the Effect of EICP Combined with Nano-SiO2 and Soil Stabilizer on Improving Loess Surface Strength. *Buildings* **2025**, *15*, 1998.
12. Chen, Y.; Hazarika, H. Extraction efficiency and activity determinants of soybean urease for sustainable biomineralization technology. *Smart Constr. Sustain. Cities* **2025**, *3*, 11. [CrossRef]
13. Lai, H.-J.; Cui, M.-J. Extraction of crude soybean urease using ethanol and its effect on soil cementation. *Soils Found.* **2023**, *63*, 101300. [CrossRef]
14. Lai, H.; Chen, Y. Extraction of high activity bacterial urease and its application to biomineralization of soil. *J. Rock Mech. Geotech. Eng.* **2025**, *17*, 1847–1861.
15. Ren, G.; Peng, Y. Rheological behavior of biogenic calcium carbonate from high-concentration enzyme-induced calcium carbonate precipitation and the mechanical properties of treated soil. *J. Rock Mech. Geotech. Eng.* **2026**, *18*, 2945–2959.
16. Cui, M.-J.; Lai, H.-J. One-phase-low-pH enzyme induced carbonate precipitation (EICP) method for soil improvement. *Acta Geotech.* **2021**, *16*, 481–489.
17. Chen, Y.-W.; Cui, M.-J. Modified one-phase-low-pH EICP method using low-pH cementation solution for soil biomineralization. *Acta Geotech.* **2025**, *20*, 4133–4146.
18. Meng, H.; Shu, S. Multiple-phase enzyme-induced carbonate precipitation (EICP) method for soil improvement. *Eng. Geol.* **2021**, *294*, 106374.
19. Huang, M.; Jiang, Q. Feasibility analysis of EICP technique for reinforcing backfill layer behind TBM tunnel linings based on model tests. *Tunn. Undergr. Space Technol.* **2025**, *155*, 106172.

20. Jiang, Q.; Huang, M. Mechanism study and optimal proportioning test of pea gravel behind TBM tunnel linings reinforcement using EICP technology. *Rock Soil Mech.* **2024**, *45*, 2037–2049.
21. Xie, J.; Zhang, H. Comparative effectiveness of MICP, EICP and EICP-lignin technologies for repairing concrete cracks of different widths. *Case Stud. Constr. Mater.* **2025**, *23*, e05659. [CrossRef]
22. Li, G.; Deng, H. Experimental study on impermeability of concrete panels repaired by Enzyme-Induced Calcium Carbonate Precipitation (EICP). *Case Stud. Constr. Mater.* **2026**, *24*, e05956. [CrossRef]
23. Chen, Y.; Tan, L. The hydro-mechanical characteristics and micro-structure of loess enhanced by microbially induced carbonate precipitation. *Geomech. Energy Environ.* **2023**, *34*, 100469.
24. Pan, C.; Zhang, C. Experimental study of urea-catalyzed microbial solution-based curing of fissured loess soil. *Front. Mater.* **2025**, *12*, 1583278.
25. Mehmood, M.; Guo, Y. Influence of Enzyme Induced Carbonate Precipitation (EICP) on the Engineering Characteristics of Expansive soil. *Arab. J. Sci. Eng.* **2024**, *49*, 14101–14116. [CrossRef]
26. Yu, B.; Dijkstra, T.A. Advanced multi-scale characterization of loess microstructure: Integrating μXCT and FIB-SEM for detailed fabric analysis and geotechnical implications. *Eng. Geol.* **2024**, *341*, 107727.
27. Luo, G.; Pan, S. Research on establishing numerical model of geo material based on CT image analysis. *EURASIP J. Image Video Process.* **2019**, *2019*, 36. [CrossRef]
28. Huang, M.; Xu, K. Effect of drying-wetting cycles on pore characteristics and mechanical properties of enzyme-induced carbonate precipitation-reinforced sea sand. *J. Rock Mech. Geotech. Eng.* **2024**, *16*, 291–302.
29. Wang, W.; He, X. Presence of Mg-calcite and its influence on MICP and EICP processes. *J. Rock Mech. Geotech. Eng.* **2025**, *17*, 5373–5384.
30. *GB/T 50123-2019*; Standard for Geotechnical Testing Method. China Planning Press: Beijing, China, 2019.
31. Ng, S.; Chu, J. Frozen enzyme EICP method for more effective soil improvement. *Acta Geotech.* **2024**, *19*, 7117–7124. [CrossRef]

Disclaimer/Publisher's Note: The statements, opinions and data contained in all publications are solely those of the individual author(s) and contributor(s) and not of MDPI and/or the editor(s). MDPI and/or the editor(s) disclaim responsibility for any injury to people or property resulting from any ideas, methods, instructions or products referred to in the content.